JACS
JOURNAL OF THE AMERICAN CHEMICAL SOCIETY

Article

pubs.acs.org/JACS

Synthetic Modularity of Protein–Metal–Organic Frameworks

Jake B. Bailey, Ling Zhang, Jerika A. Chiong, Sunhyung Ahn, and F. Akif Tezcan*

Department of Chemistry and Biochemistry, University of California at San Diego, 9500 Gilman Drive, La Jolla, California 92093, United States

Supporting Information

ABSTRACT: Previously, we adopted the construction principles of metal–organic frameworks (MOFs) to design a 3D crystalline protein lattice in which pseudospherical ferritin nodes decorated on their C_3 symmetric vertices with Zn coordination sites were connected via a ditopic benzene-dihydroxamate linker. In this work, we have systematically varied both the metal ions presented at the vertices of the ferritin nodes (Zn(II), Ni(II), and Co(II)) and the synthetic dihydroxamate linkers, which yielded an expanded library of 15 ferritin–MOFs with the expected body-centered (cubic or tetragonal) lattice arrangements. Crystallographic and small-angle X-ray scattering (SAXS) analyses indicate that lattice symmetries and dimensions of ferritin–MOFs can be dictated by both the metal and linker components. SAXS measurements on bulk crystalline samples reveal that some ferritin–MOFs can adopt multiple lattice conformations, suggesting dynamic behavior. This work establishes that the self-assembly of ferritin–MOFs is highly robust and that the synthetic modularity that underlies the structural diversity of conventional MOFs can also be applied to the self-assembly of protein-based crystalline materials.

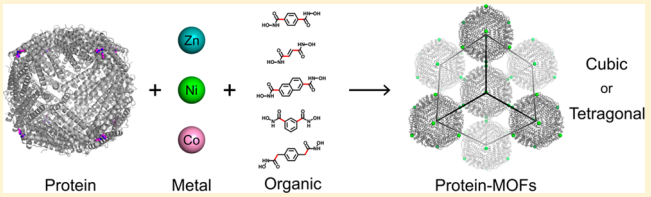

INTRODUCTION

Periodic protein arrays constitute a major component of the cellular machinery and are widely utilized as platforms for nano- and biotechnological applications due to their advanced materials properties and precise display of diverse chemical functionalities over the nm–μm scale.[1−3] Accordingly, there has been a growing interest in the construction of artificial protein assemblies.[4−7] These efforts have engendered innovative design strategies and chemical approaches, which have led to 0,[8−11] 1,[12−15] 2,[12,16−18] and 3D[19−23] assemblies with complex structures and, in some cases, sophisticated[24,25] and evolvable functions,[26] as well as emergent properties not yet observed in biology.[18,27] Despite these advances, the structural/chemical heterogeneity of proteins still poses a substantial challenge for designing supramolecular protein architectures and arrays. While most design approaches are intended to be generalizable, they still require adjustment of the protein building blocks or the self-assembly procedures on a case-by-case basis. In contrast, the thematically related field of supramolecular chemistry has benefitted from synthetic access to a large library of molecular building blocks and bonding strategies,[28,29] which can be mixed and matched to create structural and functional diversity with relative ease. Such synthetic versatility is aptly highlighted by metal–organic frameworks (MOFs),[30−40] a vast class of crystalline materials composed of metal-based nodes and organic linkers that can be combined in a modular fashion.

We recently adopted the construction strategies of MOFs to create 3D protein lattices in which pseudospherical ferritin molecules decorated on their outer surfaces with metal coordination sites were bridged via ditopic metal-chelating linkers (benzene-1,4-dihydroxamic acid; *p*-H_2bdh or **1**; Figure 1b).[41] Despite the remarkable size mismatch between the *p*-H_2bdh linkers (ca. 9 Å long, 196 g/mol) and ferritin nodes (120 Å across, >505 000 g/mol), their interactions were sufficiently strong to dictate the arrangement of ferritin molecules into the desired body-centered cubic (bcc) lattice. This system introduced a new class of tripartite hybrid materials whose self-assembly is dependent on each of its components: protein, metal, and organic linker. In this study, we set out to examine if the modularity that is inherent in conventional MOFs and renders them particularly attractive as functional materials also applies to protein–MOFs. Specifically, we asked whether it is possible to synthetically modulate the formation and structural parameters of protein–MOFs through discrete molecular interactions.

RESULTS AND DISCUSSION

Construction of Ferritin–MOF Components. *Metal–Ferritin Nodes.* To enable a modular construction approach, we sought to diversify the metal and the organic linker components of the ferritin–MOFs (Figure 1). As previously described,[41] the 24meric human heavy-chain ferritin (which we refer to as ferritin in this report) provides an attractive building block for protein–MOFs for two primary reasons. First, from a structural perspective, ferritin possesses an octahedral (432) symmetry reminiscent of many metal nodes employed in archetypal MOFs,[42,43] which could, in principle, provide access to different lattice arrangements (e.g., simple, face-centered and body-centered cubic) depending on the surface location of engineered metal binding sites. Second,

Received: February 3, 2017

DOI: 10.1021/jacs.7b01202
J. Am. Chem. Soc. XXXX, XXX, XXX–XXX

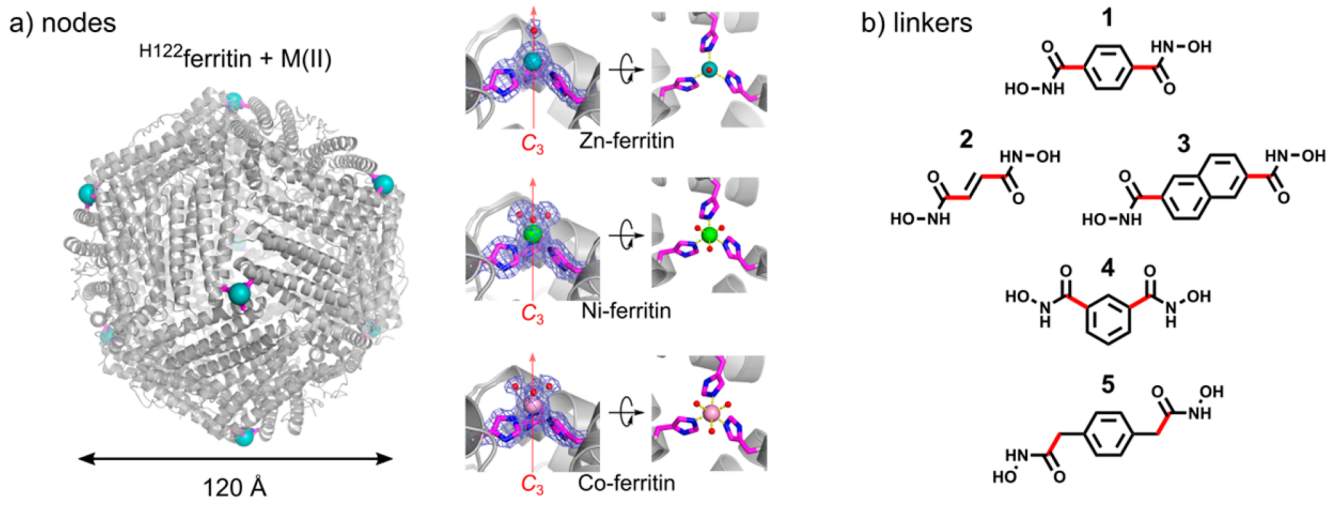

Figure 1. Modular components of ferritin–MOFs. (a) The ferritin node (metal ions at the C_3 vertices are shown as teal spheres). Close-up views of the Zn(II), Ni(II), and Co(II) coordination environments. Water molecules are shown as red spheres. $2F_o–F_c$ maps are contoured to 1σ. (b) Ditopic hydroxamic acid linkers.

ferritin is inherently functional and catalyzes iron biomineralization in its hollow interior (8 nm in diameter). The native ability of ferritin to act as a molecular template and container has in fact been exploited in numerous applications.[44−50] We previously showed that, upon assembly into MOFs, the ferritin nodes are still capable of iron mineralization, whereby the high lattice porosity allows for rapid diffusion of Fe and its uptake into the individual ferritin nodes, likely through the C_4 symmetric pores.[41,51]

In our initial studies, we deemed the C_3 symmetric pores of ferritin (essentially the eight vertices of a cube) as the most suitable locations for the installment of metal anchoring sites (Figure 1a). These corner locations allow for the installment of surface-exposed tripodal coordination motifs that can bind various metal ions with high affinity, while still presenting outward-facing open coordination sites available for organic linkers. While the C_4 symmetric pores also permit stable, square planar metal anchoring sites to be built, the appropriate positions (residue 173 or 165) in these pores are somewhat recessed from the protein surface and therefore not immediately available as connection points for organic linkers. Technically, tri- or tetradentate coordination sites could also be incorporated onto the C_2 symmetric surfaces of ferritin, but this would require extensive design and engineering and result in multiple metal binding sites on the same surface. To build metal anchoring sites at the C_3 symmetric pores, Thr122 residues lining the outer rim of these pores were replaced with His. In our previous study, we established that the resulting variant (^{T122H}ferritin) bound Zn(II) ions in the expected tetrahedral geometry with a tripodal base of three His side chains and a single, solvent-bound coordination site pointing to the protein exterior (Figures 1a and S1).[41] We will hereafter refer to this ferritin variant as Zn–ferritin.

In this study, we prepared the Ni– and Co–adducts of ^{T122H}ferritin (Ni– and Co–ferritin) in a similar fashion as Zn–ferritin (Table S1), whereby a large molar excess of Ni(II) or Co(II) was added to ferritin solutions to saturate all available metal binding sites within the protein cage, including the installed tripodal coordination motifs at the C_3 vertices. Ni– and Co–ferritin were crystallized by vapor diffusion in the presence of Ca^{2+}, which selectively induces the formation of face-centered cubic (fcc; *F*432 space group) lattices by joining ferritin molecules across their C_2 symmetric interfaces via coordination to pairs of D84 and engineered Q86 residues.[52] The crystal structures of Ni– and Co–ferritin were determined at 1.79 and 1.95 Å resolution, respectively (Table S2; PDB IDs: 5UP7 and 5VTD). These structures confirm that Ni(II) and Co(II) ions are anchored by the tripodal H122 coordination motifs at full occupancy, with three aquo ligands completing nearly ideal octahedral coordination spheres. Relative to the tetrahedral Zn coordination sites in Zn–ferritin, in Ni– and Co–ferritin, the His122 side chains have moved slightly to accommodate the octahedral geometry, with $N_{His}–M–N_{His}$ angles of 95°–96°, $N_{His}–M–OH_2$ angles of 94° (Ni) and 87° (Co), and $OH_2–M–OH_2$ angles of 75° (Ni) and 82° (Co). The $M–N_{His}$ distances are 2.1 Å for both species, and the $M–OH_2$ distances are 2.1 Å for Ni–ferritin and 2.2 Å for Co–ferritin. These observations thus establish that Ni– and Co–ferritin nodes are poised for coordinating bridging linkers.

Synthetic Linkers. With the three distinct metallo–ferritin nodes in hand, we next prepared a set of five ditopic ligands (**1**–**5**) bearing hydroxamic acid head groups (Figure 1b), which have been previously reported.[41,53−56] For the synthesis of ligands **1** and **4** (benzene-1,3-dihydroxamic acid; *m*-H_2bdh), we followed published protocols.[41,53] Ligands **2** (*E*-ethylenedihydroxamic acid or *E*-H_2edh), **3** (naphthalene-2,6-dihydroxamic acid or 2,6-H_2ndh), and **5** (xylene-1,4-dihydroxamic acid or *p*-H_2xdh) were prepared by the amidation of the respective dicarboxylate-bearing precursors with *O*-tritylhydroxylamine, followed by deprotection with trifluoroacetic acid to furnish the dihydroxamic acid ligands (see the Supporting Information for details on linker synthesis and characterization). Hydroxamate functionalities were chosen due to their high affinity for Zn(II), Ni(II), and Co(II), as well as their sterically unencumbered nature compared to other commonly used aromatic chelates (e.g., polypyridyl or catecholate-type ligands), allowing for unhindered access to the surface-anchored metal ions without bias from peripheral contacts.

The primary differences between ligands **1**–**5** can be described by two parameters. First, the interhydroxamate spacing (i.e., the linker length) of these ligands ranges from <7.0 Å in **2** to >11 Å in **3** and **5**. Second, the ligands offer four

DOI: 10.1021/jacs.7b01202
J. Am. Chem. Soc. XXXX, XXX, XXX–XXX

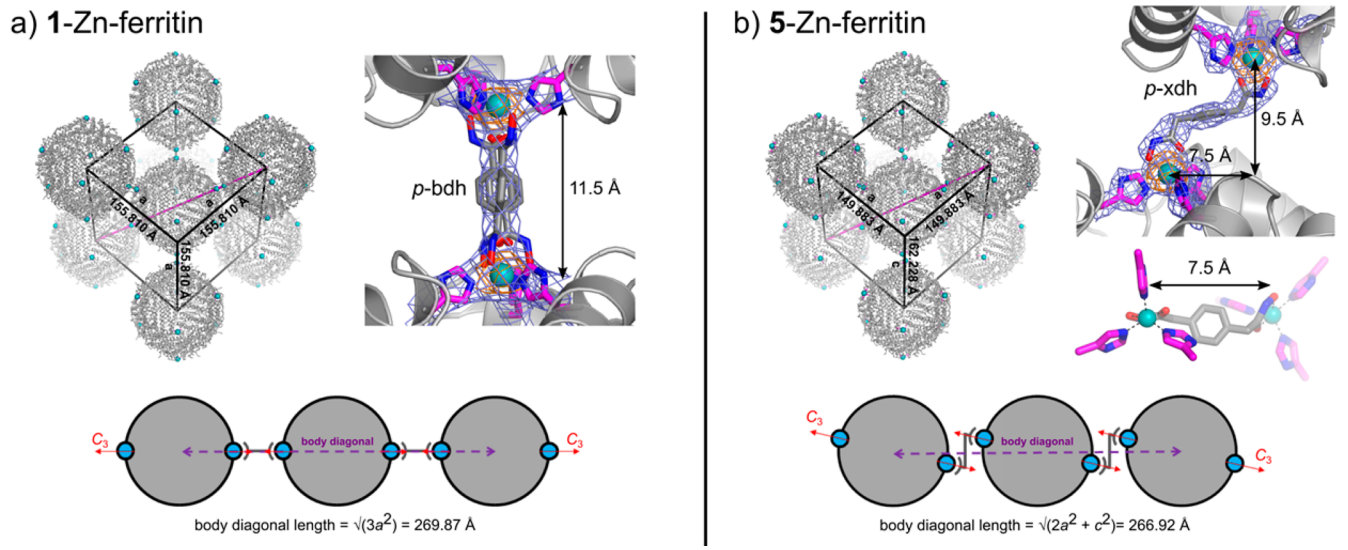

Figure 2. sc-XRD structures for (a) **1**−Zn−ferritin and (b) **5**−Zn−ferritin. Zinc atoms are highlighted as teal spheres. $2F_o-F_c$ electron density maps are contoured at 1σ (blue) and 3σ (orange). The body diagonals of the unit cells are shown as purple lines.

different geometries in terms of the relative orientations of the two hydroxamate head groups. Here, we define these orientations with respect to the vector along the C−C bond (highlighted in red in Figures 1b and S1) that appends the hydroxamate moieties to the core of each ligand. In **1**, the bond vectors are collinear; in **2** and **3**, they are parallel but offset; and in **4**, they form an obtuse angle. Finally, in **5**, the vectors are not fixed due to the rotational degrees of freedom about the methylene spacers: they can yield parallel or bent orientations but not collinear. Ligand **5** thus offers another variation among the five linkers, namely increased conformational flexibility.

Self-Assembly of Ferritin−MOFs and Crystallographic Characterization. Under previously established self-assembly conditions,[41] all 15 combinations of the three ferritin nodes (Zn−ferritin, Ni−ferritin, and Co−ferritin) and five organic linkers reproducibly yielded single-crystalline particles with rhombic dodecahedral morphology (Figure S2). Self-assembly of the crystalline lattices occurred within 12−24 h in aqueous solutions containing 4.2 μM ferritin, 72 equiv (per 24meric ferritin cage) of Zn(II), Ni(II), or Co(II) and 2 mM organic linker at pH 9.5 and 23 °C. The sizes of these crystals ranged from 5 to 200 μm. No crystals formed when any of the three components (ferritin, metal, or linker) was omitted from the self-assembly solutions, providing strong evidence for the tripartite composition of the crystal lattices.

To understand the assembly of ferritin−MOFs in detail and to examine the relationship between lattice symmetry and metal/linker geometry, we pursued single-crystal X-ray diffraction (sc-XRD) experiments. Ferritin−MOFs pose a unique challenge in this regard in that the constituent building blocks are very large molecules bridged by small linkers with inherent flexibility and exceedingly small interaction footprints. In terms of node/linker mass ratios, ferritin−MOFs (ca. 2500/1) are akin to a lattice of regulation-size soccer balls held together by wooden toothpicks. Remarkably, the total footprint of hydroxamate−metal interactions (ca. 22 Å^2 × 8 in bcc arrangement) represents only 0.4% of the outer surface of a ferritin cage (ca. 44,000 Å^2). In a densely packed protein crystal like that of the globular protein sperm whale myoglobin (PDB ID: 5IKS, solvent content = 0.35), the fraction of the total protein surface area engaged in lattice packing contacts is 16%. In the case of a sparsely packed protein crystal (PDB ID: 1B5S, solvent content = 0.89), this fraction is 8%, that is, 20-fold higher than in ferritin−MOFs (PDB ID: 5CMR, solvent content = 67%). These comparisons intimate that the ferritin−MOFs should be quite dynamic and highly sensitive to external perturbations and, at first glance, not conducive to high-resolution structure determination by sc-XRD. Earlier screening efforts led to single crystals of **1**−Zn−ferritin which diffracted to 3.8-Å resolution at best, with the great majority diffracting to >6.0 Å.[41] Here, we carried out a broader screen of the self-assembly conditions, which enabled us to obtain midresolution sc-XRD data for two ferritin−MOF variants and determine their crystal structures (Table S1): **1**−Zn−ferritin (improved from 3.8 to 2.63 Å resolution, *I*432, a = 155.8 Å; PDB ID: 5UP8) and **5**−Zn−ferritin (2.45 Å resolution, *I*4, a = 149.88 Å, c = 162.23 Å; PDB ID: 5UP9).

In the bcc crystals of **1**−Zn−ferritin, the C_3 symmetry axes of the individual ferritin molecules are perfectly aligned with the crystallographic 3-fold symmetry axes that form the body diagonals in the unit cells (Figure 2a). Consequently, the length of each body diagonal (269.9 Å) is the sum of the diameters of two ferritin molecules (i.e., 2 × 123.4 Å, as measured by the distance between two Zn ions along the C_3 axis within each ferritin molecule) and twice the separation between the Zn ions across the linker-mediated interface (i.e., 2 × 11.5 Å). Owing to the cubic symmetry, each linker **1** is centered precisely at the intersection of the crystallographic 2- and 3-fold symmetry axes. This positioning, combined with the rotational averaging of linker **1** about the 3-fold axis, gives rise to a diffuse electron density for the linker, even at the considerably improved resolution limit (Figure 2a).

These complications are eliminated in the case of the body-centered tetragonal (bct) lattices of **5**−Zn−ferritin which lack crystallographic 3-fold symmetry and therefore present a unique orientation of linker **5** between the two crystallographically nonequivalent Zn centers (Figure 2b). The resultant, well-defined electron density allowed us to build an unambiguous structural model of linker **5** and the Zn coordination environments. This model confirms that the hydroxamate head groups bind the Zn centers in a bidentate geometry in the apical position, completing a pseudotetrahedral

DOI: 10.1021/jacs.7b01202
J. Am. Chem. Soc. XXXX, XXX, XXX−XXX

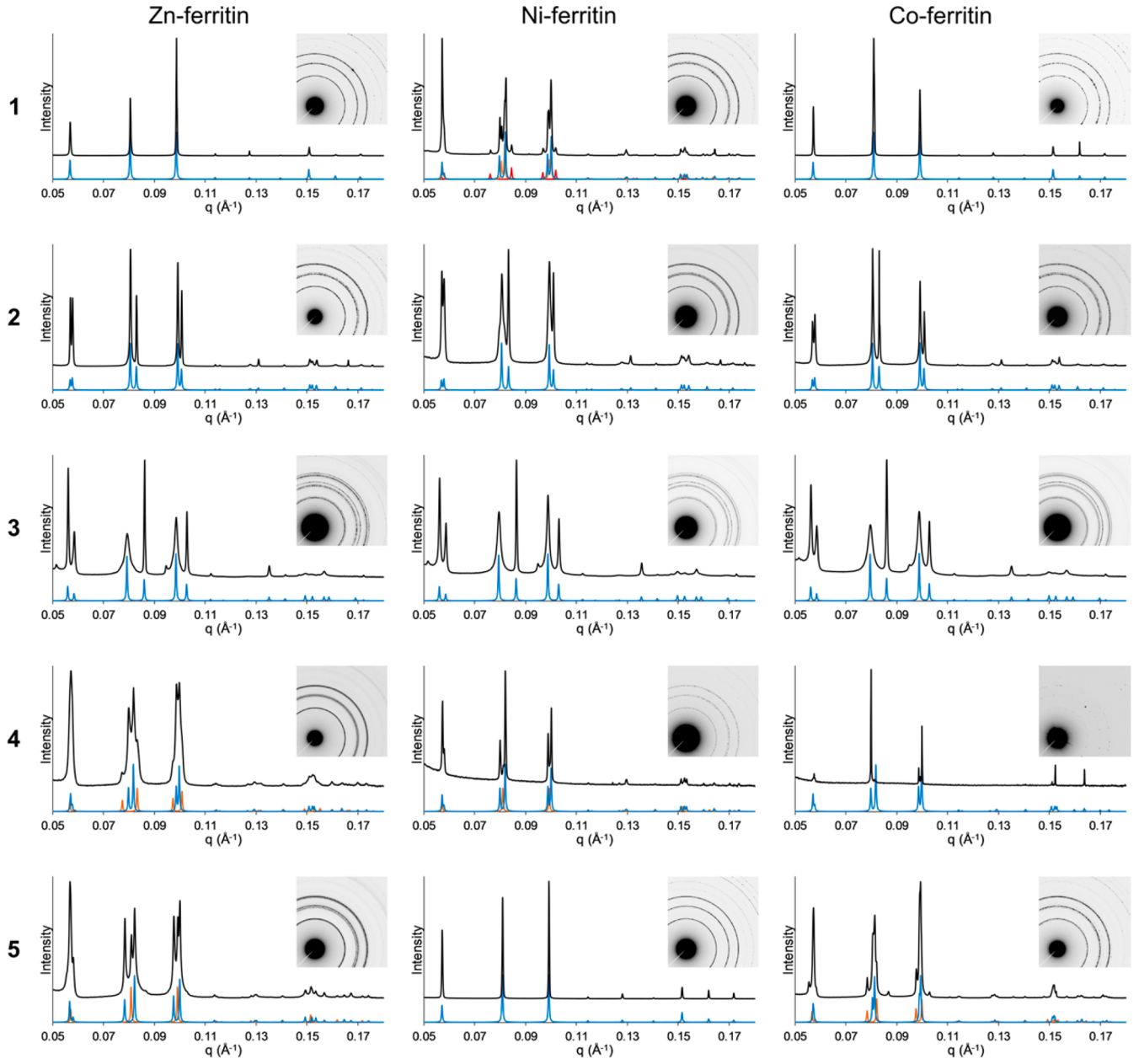

Figure 3. SAXS profiles of Zn−, Ni−, and Co−ferritin−MOFs mediated by linkers **1**−**5**. Simulated diffraction patterns of the primary lattice are shown in blue. Simulated patterns for any additional lattices are shown in orange or red. See Table 1 for the lattice parameters.

Zn coordination geometry, with both Fe−O coordination distances at 2.2 Å. The xylene moiety of the linker assumes a nearly parallel orientation with respect to the ferritin−ferritin interfacial plane, giving rise to a large (ca. 3.75 Å) lateral displacement of the Zn ions from the body diagonal of the bct unit cell, thereby yielding a considerable cubic-to-tetragonal distortion (Figure 2b). Due to the flat orientation of the linker, the interfacial spacing between the ferritin molecules (as defined by the projected Zn−Zn distance) is reduced to 9.5 Å from 11.5 Å observed in the cubic **1**−Zn−ferritin lattices (Figure 2). This compaction brings a small number of interfacial side chains into a distance range (3.8−5 Å) where electrostatic interactions between ferritin molecules may be invoked (Figure S3). However, based on our observation that all three components of ferritin−MOFs are necessary to form crystalline lattices and the fact that body-centered lattices (i.e., *I*432 and *I*4) have otherwise not been observed with human heavy-chain ferritin, we can safely conclude that linker-mediated interactions are the driving force for the formation of the observed ferritin−MOF lattices.

Characterization of Ferritin−MOFs by Small-Angle X-ray Scattering. Although sc-XRD experiments can provide highly detailed structural information, they also require atomic-level registry between the constituents of a lattice, which can be challenging to achieve in the case of ferritin−MOFs. Yet, as the cartoons in Figure 2 illustrate, there is a rather simple relationship between the crystallographic parameters of ferritin−MOFs (i.e., symmetry and unit cell parameters) and the linker-mediated protein−protein interactions. Thus, we turned to small-angle X-ray scattering (SAXS) experiments which can furnish the desired crystallographic parameters without the need for sc-XRD-quality crystals and enable bulk measurements that can help identify any heterogeneity in the

DOI: 10.1021/jacs.7b01202
J. Am. Chem. Soc. XXXX, XXX, XXX−XXX

Table 1. Unit Cell Parameters for Ferritin−MOFs Shown in Figure 3

	Zn−ferritin		Ni−ferritin		Co−ferritin	
Linker	Symmetry	Unit Cell	Symmetry	Unit Cell	Symmetry	Unit Cell
1	Cubic *I*	a = 155.97 Å	Tetragonal *I*	a = 152.89 Å, c = 157.48 Å	Cubic *I*	a = 155.23 Å
			Tetragonal *I*[a]	a = 153.51 Å, c = 155.91 Å		
			Tetragonal *I*[b]	a = 148.58 Å, c = 164.92 Å		
2	Tetragonal *I*	a = 155.90 Å, c = 151.36 Å	Tetragonal *I*	a = 155.77 Å, c = 150.74 Å	Tetragonal *I*	a = 156.01 Å, c = 151.18 Å
3	Tetragonal *I*[c]	a = 158.45 Å, c = 145.93 Å	Tetragonal *I*[c]	a = 158.05 Å, c = 145.46 Å	Tetragonal *I*[c]	a = 157.81 Å, c = 146.00 Å
4	Tetragonal *I*	a = 153.53 Å, c = 157.26 Å	Tetragonal *I*	a = 153.11 Å, c = 157.02 Å	Tetragonal *I*	a = 153.50 Å, c = 157.28 Å
	Tetragonal *I*[a]	a = 150.76 Å, c = 162.08 Å	Cubic *I*[a]	a = 154.86 Å		
5	Tetragonal *I*	a = 152.67 Å, c = 160.27 Å	Cubic *I*	a = 155.16 Å	Tetragonal *I*	a = 154.44 Å, c = 156.05 Å
	Cubic *I*[a]	a = 155.24 Å			Tetragonal *I*[a]	a = 152.85 Å, c = 160.19 Å

[a]Simulated SAXS pattern is shown in orange in Figure 3. [b]Simulated SAXS pattern is shown in red in Figure 3. [c]The additional peaks observed for **3**−M−ferritin could be indicative of a primitive (*P*) tetragonal unit cell (see Figure S4).

crystalline samples which would be missed in sc-XRD experiments.

All 15 ferritin MOFs produced well-defined SAXS patterns (Figure 3), which allowed us to determine their lattice symmetries and unit cell parameters (Table 1). All variants possess bcc (cubic *I*) and/or bct (tetragonal *I*) symmetry and possess unit cell dimensions that fall within 155 ± 10 nm. These observations establish that each ferritin−MOF is formed through the desired linker-mediated association of the metal centers at the C_3 vertices of ferritin nodes. Indeed, when the metal-bound ferritins are treated with Ca^{2+} instead of the linkers, a clear SAXS pattern for an fcc lattice is produced (Figure S5), demonstrating the chemical selectivity of linker-mediated ferritin self-assembly. To assess the accuracy of the SAXS measurements, we compared the unit cell parameters of **1**−Zn−ferritin determined by SAXS (bcc, a = 155.97 Å) to those derived from sc-XRD (a = 155.81 Å), which revealed a close correspondence between the two types of measurements.

An initial inspection of the SAXS data indicates that bulk samples of most ferritin−MOF variants (10) consist of single, body-centered lattices. However, certain metal/ligand combinations (5) yield at least two distinct lattices (shown in different colors in Figure 3 and separately listed in Table 1), consistent with the expectation that ferritin−MOFs may be inherently flexible and that subtle changes in the metal-linker coordination and linker geometry can give rise to measurable changes in the lattice parameters. The most prominent example is provided by the simultaneous observation of three distinct bct lattices of **1**−Ni−ferritin whose unit cell parameters vary by ca. 7% (mean dimension: 154.3 ± 10.0 Å). This variation points to different extents of tetragonal distortion, i.e., the difference between the a and c dimensions which is related to the displacement of the linker-bound metal ions from the body diagonals (see Figure S6 for structural models). In the bulk samples of **4**−Ni− and **5**−Zn−ferritin crystals, both tetragonal and cubic lattices are observed, meaning that the flexibility in the linker geometry can allow the ferritin C_3 axes to align with or deviate from the body diagonals. It must be noted that the unit cell parameters for the tetragonal sublattice of **5**−Zn−ferritin determined by room-temperature SAXS experiments (a = 152.67 Å, c = 160.27 Å) show a smaller tetragonal distortion compared to the sc-XRD case (a = 149.88 Å, c = 162.23 Å). This points to a reduced lateral displacement and a ca. 1.1-Å longer interfacial separation (projected Zn−Zn distance estimated to be ca. 10.5 Å), which could be readily accommodated by the tilting of linker **5** with respect to the interfacial plane and bond rotations about the methylene spacers (Figure S7). At this interfacial separation, there would be no direct protein−protein contacts, suggesting that the crystallographically observed interprotein contacts are a consequence of the cryogenic temperatures used in sc-XRD experiments.

A closer examination of the SAXS data reveals some trends related to the metal and linker components of ferritin MOFs. First, Zn− and Co−ferritin−MOF lattices are nearly identical to one another in almost all instances but distinct from Ni−ferritin−MOFs in the case of linkers **1**, **4**, and **5**. Whereas linker **1** yields exclusively a cubic lattice with Zn− and Co−ferritin, it produces tetragonal symmetry with Ni−ferritin. While the primary lattices are nearly identical for linker **4**, only the Ni−ferritin forms an additional cubic lattice. The opposite trend is observed with linker **5**, where Ni−ferritin forms a single cubic lattice while Zn− and Co−ferritin form a similar cubic (or near cubic) lattice as well as a tetragonal lattice.

These observations can be ascribed to the similarities between Zn(II) and Co(II) in terms of their coordination preferences for a tetrahedral geometry (as well as similar ionic radii and reactivity patterns),[57] whereas Ni(II) typically tends toward higher coordination numbers and octahedral geometry. Thus, at least in some ferritin−MOF variants, the specific combination of metal coordination geometry and the linker structure dictate distinct outcomes in terms of the lattice architecture. In the case of linker **1**, we can propose a structural model in which Zn(II) or Co(II) centers would accommodate a

DOI: 10.1021/jacs.7b01202
J. Am. Chem. Soc. XXXX, XXX, XXX−XXX

head-on (apical) hydroxamate coordination to complete a pseudotetrahedral geometry. This geometry, combined with the linearity of linker **1**, would align the C_3 axes of the connected ferritin nodes to yield cubic lattice symmetry, as observed in the crystal structure of **1**−Zn−ferritin. In contrast, for Ni−ferritin, whose octahedral Ni(II) centers would prefer a "side-on" attachment by the hydroxamate moiety, the linear linker **1** would offset the ferritin C_3 axes to yield a tetragonal lattice (Figure S6). Conversely, the "bent" linker **4** could yield a cubic or tetragonal lattice symmetry through side-on Ni(II) coordination, while the apical Zn(II) and Co(II) coordination leads to a tetragonal lattice. Such models are more difficult to propose for linker **5**, whose inherently higher flexibility could be expected to dampen the influence of metal−hydroxamate coordination geometry on the lattice structure. Regardless, further sc-XRD characterization will be necessary to probe the validity of these structural models.

Interestingly, linkers **2** and **3** always yield tetragonal lattices regardless of the metal component they are paired with. Since these two ligands display the same relative hydroxamate orientations ("parallel but offset"), they also provide a valid point of comparison in terms of how the linker dimensions affect lattice metrics. Indeed, we observe that the longer linker **3** consistently produces a larger tetragonal distortion ($|a - c| \geq 11.8$ Å) than **2** ($|a - c| \leq 5.0$ Å) for all metallo−ferritin nodes. These observations indicate that synthetic linkers can also modulate the unit cell dimensions of ferritin−MOFs.

CONCLUSIONS

Here we have reported the construction and characterization of a large library of 3D, crystalline protein−MOFs through a combination of three different metallo−ferritin nodes and five synthetic linkers bearing hydroxamate head groups. Our results establish that the metal ion and the synthetic linker components can be varied in a modular fashion to influence the structural parameters (i.e., lattice symmetries and unit cell dimensions) of protein−MOFs, akin to conventional MOFs. Despite the remarkable size discrepancy between the ferritin nodes and the organic linkers, the self-assembly of the ferritin−MOFs is highly robust, emphasizing the utility of metal coordination interactions in controlling protein self-assembly. Excitingly, by virtue of the flexibility of the linkers and/or the fluxionality of metal-linker bonds, several ferritin−MOFs have been observed to adopt multiple lattice conformations, which suggests that they may display dynamic behavior. Some of our immediate goals include the utilization of linkers whose lengths approximate the dimensions of the protein nodes and investigating the emergent functional/physical properties of protein−MOFs (e.g., their potential dynamic nature) arising from their unique, tripartite composition.

ASSOCIATED CONTENT

Supporting Information

The Supporting Information is available free of charge on the ACS Publications website at DOI: 10.1021/jacs.7b01202.

Additional experimental details (Materials and Methods), tables (Supporting Tables 1 and 2), and figures (Supporting Figures 1−18) (PDF)

AUTHOR INFORMATION

Corresponding Author

*tezcan@ucsd.edu

ORCID

F. Akif Tezcan: 0000-0002-4733-6500

Notes

The authors declare no competing financial interest.

ACKNOWLEDGMENTS

We thank Drs. Milan Gembicky, Curtis Moore, and Steven Weigand for assistance with sc-XRD and SAXS measurements. This work was primarily funded by the U.S. DOE (BES, Division of Materials Sciences, Biomolecular Materials Program, DE-FG02-10ER46677 to F.A.T.). Additional support was provided by NSF (ligand synthesis, DMR-1602537 to F.A.T.) Crystallographic data were collected at SSRL, supported by the U.S. DOE (Office of Science, BES and BER), as well as by the NIH. SAXS experiments were performed at APS, a DOE Office of Science User Facility operated by Argonne National Laboratory under Contract No. DE-AC02-06CH11357.

REFERENCES

(1) Mann, S. *Angew. Chem., Int. Ed.* **2008**, *47* (29), 5306−5320.
(2) Yang, L.; Liu, A.; Cao, S.; Putri, R. M.; Jonkheijm, P.; Cornelissen, J. J. *Chem. - Eur. J.* **2016**, *22* (44), 15570−15582.
(3) Ueno, T. *Chem. - Eur. J.* **2013**, *19* (28), 9096−9102.
(4) Yeates, T. O.; Liu, Y.; Laniado, J. *Curr. Opin. Struct. Biol.* **2016**, *39*, 134−143.
(5) Kobayashi, N.; Arai, R. *Curr. Opin. Biotechnol.* **2017**, *46*, 57−65.
(6) Salgado, E. N.; Radford, R. J.; Tezcan, F. A. *Acc. Chem. Res.* **2010**, *43* (5), 661−672.
(7) Radford, R. J.; Brodin, J. D.; Salgado, E. N.; Tezcan, F. A. *Coord. Chem. Rev.* **2011**, *255* (7−8), 790−803.
(8) Lai, Y.-T.; Hura, G. L.; Dyer, K. N.; Tang, H. Y.; Tainer, J. A.; Yeates, T. O. *Sci. Adv.* **2016**, *2* (12), e1501855.
(9) King, N. P.; Bale, J. B.; Sheffler, W.; McNamara, D. E.; Gonen, S.; Gonen, T.; Yeates, T. O.; Baker, D. *Nature* **2014**, *510* (7503), 103−108.
(10) Sciore, A.; Su, M.; Koldewey, P.; Eschweiler, J. D.; Diffley, K. A.; Linhares, B. M.; Ruotolo, B. T.; Bardwell, J. C.; Skiniotis, G.; Marsh, E. N. G. *Proc. Natl. Acad. Sci. U. S. A.* **2016**, *113* (31), 8681−8686.
(11) Ni, T. W.; Tezcan, F. A. *Angew. Chem., Int. Ed.* **2010**, *49* (39), 7014−7018.
(12) Brodin, J. D.; Ambroggio, X. I.; Tang, C. Y.; Parent, K. N.; Baker, T. S.; Tezcan, F. A. *Nat. Chem.* **2012**, *4* (5), 375−382.
(13) Brodin, J. D.; Smith, S. J.; Carr, J. R.; Tezcan, F. A. *J. Am. Chem. Soc.* **2015**, *137* (33), 10468−10471.
(14) Yang, G.; Zhang, X.; Kochovski, Z.; Zhang, Y.; Dai, B.; Sakai, F.; Jiang, L.; Lu, Y.; Ballauff, M.; Li, X. *J. Am. Chem. Soc.* **2016**, *138* (6), 1932−1937.
(15) Ballister, E. R.; Lai, A. H.; Zuckermann, R. N.; Cheng, Y.; Mougous, J. D. *Proc. Natl. Acad. Sci. U. S. A.* **2008**, *105* (10), 3733−3738.
(16) Sinclair, J. C.; Davies, K. M.; Venien-Bryan, C.; Noble, M. E. M. *Nat. Nanotechnol.* **2011**, *6* (9), 558−562.
(17) Gonen, S.; DiMaio, F.; Gonen, T.; Baker, D. *Science* **2015**, *348* (6241), 1365−1368.
(18) Suzuki, Y.; Cardone, G.; Restrepo, D.; Zavattieri, P. D.; Baker, T. S.; Tezcan, F. A. *Nature* **2016**, *533* (7603), 369−373.
(19) Lanci, C. J.; MacDermaid, C. M.; Kang, S.-g.; Acharya, R.; North, B.; Yang, X.; Qiu, X. J.; DeGrado, W. F.; Saven, J. G. *Proc. Natl. Acad. Sci. U. S. A.* **2012**, *109* (19), 7304−7309.
(20) Sakai, F.; Yang, G.; Weiss, M. S.; Liu, Y.; Chen, G.; Jiang, M. *Nat. Commun.* **2014**, *5*, 4634.
(21) Künzle, M.; Eckert, T.; Beck, T. *J. Am. Chem. Soc.* **2016**, *138* (39), 12731−12734.
(22) Kostiainen, M. A.; Hiekkataipale, P.; Laiho, A.; Lemieux, V.; Seitsonen, J.; Ruokolainen, J.; Ceci, P. *Nat. Nanotechnol.* **2012**, *8* (1), 52−56.

DOI: 10.1021/jacs.7b01202
J. Am. Chem. Soc. XXXX, XXX, XXX−XXX

(23) Radford, R. J.; Lawrenz, M.; Nguyen, P. C.; McCammon, J. A.; Tezcan, F. A. *Chem. Commun.* **2011**, *47* (1), 313−315.
(24) Joh, N. H.; Wang, T.; Bhate, M. P.; Acharya, R.; Wu, Y.; Grabe, M.; Hong, M.; Grigoryan, G.; DeGrado, W. F. *Science* **2014**, *346* (6216), 1520−1524.
(25) Votteler, J.; Ogohara, C.; Yi, S.; Hsia, Y.; Nattermann, U.; Belnap, D. M.; King, N. P.; Sundquist, W. I. *Nature* **2016**, *540* (7632), 292−295.
(26) Song, W. J.; Tezcan, F. A. *Science* **2014**, *346* (6216), 1525−1528.
(27) Brodin, J. D.; Carr, J. R.; Sontz, P. A.; Tezcan, F. A. *Proc. Natl. Acad. Sci. U. S. A.* **2014**, *111* (8), 2897−2902.
(28) Chakrabarty, R.; Mukherjee, P. S.; Stang, P. J. *Chem. Rev.* **2011**, *111* (11), 6810−6918.
(29) Corbett, P. T.; Leclaire, J.; Vial, L.; West, K. R.; Wietor, J.-L.; Sanders, J. K. M.; Otto, S. *Chem. Rev.* **2006**, *106* (9), 3652−3711.
(30) Furukawa, H.; Cordova, K. E.; O'Keeffe, M.; Yaghi, O. M. *Science* **2013**, *341* (6149), 1230444.
(31) Zhou, H.-C.; Kitagawa, S. *Chem. Soc. Rev.* **2014**, *43* (16), 5415−5418.
(32) Eddaoudi, M.; Kim, J.; Rosi, N.; Vodak, D.; Wachter, J.; O'Keeffe, M.; Yaghi, O. M. *Science* **2002**, *295* (5554), 469−472.
(33) Howarth, A. J.; Peters, A. W.; Vermeulen, N. A.; Wang, T. C.; Hupp, J. T.; Farha, O. K. *Chem. Mater.* **2017**, *29* (1), 26−39.
(34) Chui, S. S.-Y.; Lo, S. M.-F.; Charmant, J. P. H.; Orpen, A. G.; Williams, I. D. *Science* **1999**, *283* (5405), 1148−1150.
(35) Li, J. R.; Sculley, J.; Zhou, H. C. *Chem. Rev.* **2012**, *112* (2), 869−932.
(36) Horike, S.; Shimomura, S.; Kitagawa, S. *Nat. Chem.* **2009**, *1* (9), 695−704.
(37) Yoon, M.; Srirambalaji, R.; Kim, K. *Chem. Rev.* **2012**, *112* (2), 1196−1231.
(38) Sumida, K.; Rogow, D. L.; Mason, J. A.; McDonald, T. M.; Bloch, E. D.; Herm, Z. R.; Bae, T. H.; Long, J. R. *Chem. Rev.* **2012**, *112* (2), 724−781.
(39) Horcajada, P.; Gref, R.; Baati, T.; Allan, P. K.; Maurin, G.; Couvreur, P.; Ferey, G.; Morris, R. E.; Serre, C. *Chem. Rev.* **2012**, *112* (2), 1232−1268.
(40) Wang, Z.; Cohen, S. M. *Chem. Soc. Rev.* **2009**, *38* (5), 1315−1329.
(41) Sontz, P. A.; Bailey, J. B.; Ahn, S.; Tezcan, F. A. *J. Am. Chem. Soc.* **2015**, *137* (36), 11598−11601.
(42) Li, H.; Eddaoudi, M.; O'Keeffe, M.; Yaghi, O. M. *Nature* **1999**, *402* (6759), 276−279.
(43) Barthelet, K.; Marrot, J.; Riou, D.; Ferey, G. *Angew. Chem., Int. Ed.* **2002**, *41* (2), 281−284.
(44) Abe, S.; Ueno, T. *RSC Adv.* **2015**, *5* (27), 21366−21375.
(45) MaHam, A.; Tang, Z. W.; Wu, H.; Wang, J.; Lin, Y. H. *Small* **2009**, *5* (15), 1706−1721.
(46) Meldrum, F. C.; Heywood, B. R.; Mann, S. *Science* **1992**, *257* (5069), 522−524.
(47) Abe, S.; Niemeyer, J.; Abe, M.; Takezawa, Y.; Ueno, T.; Hikage, T.; Erker, G.; Watanabe, Y. *J. Am. Chem. Soc.* **2008**, *130* (32), 10512−10514.
(48) Aime, S.; Frullano, L.; Geninatti Crich, S. *Angew. Chem., Int. Ed.* **2002**, *41* (6), 1017−1019.
(49) Butts, C. A.; Swift, J.; Kang, S.-g.; Di Costanzo, L.; Christianson, D. W.; Saven, J. G.; Dmochowski, I. J. *Biochemistry* **2008**, *47* (48), 12729−12739.
(50) Swift, J.; Wehbi, W. A.; Kelly, B. D.; Stowell, X. F.; Saven, J. G.; Dmochowski, I. J. *J. Am. Chem. Soc.* **2006**, *128* (20), 6611−6619.
(51) Bernacchioni, C.; Ghini, V.; Theil, E. C.; Turano, P. *RSC Adv.* **2016**, *6*, 21219−21227.
(52) Lawson, D. M.; Artymiuk, P. J.; Yewdall, S. J.; Smith, J. M.; Livingstone, J. C.; Treffry, A.; Luzzago, A.; Levi, S.; Arosio, P.; Cesareni, G.; Thomas, C. D.; Shaw, W. V.; Harrison, P. M. *Nature* **1991**, *349* (6309), 541−4.
(53) Bai, Y.; Guo, D.; Duan, C. Y.; Dang, D. B.; Pang, K. L.; Meng, Q. J. *Chem. Commun.* **2004**, *2*, 186−187.
(54) Breslow, R.; Jursic, B.; Yan, Z. F.; Friedman, E.; Leng, L.; Ngo, L. *Proc. Natl. Acad. Sci. U. S. A.* **1991**, *88*, 5542−5546.
(55) Yamaye, M.; Nago, Y.; Sasaki, M.; Tsuru, T.; Mukae, K.; Yoshinaga, T.; Murayama, R.; Tahara, C. *Polym. Degrad. Stab.* **2006**, *91*, 2014−2021.
(56) Saxena, N.; Juneja, H. D.; Munshi, K. N. *J. Indian Chem. Soc.* **1993**, *70* (11−12), 943−949.
(57) Bertini, I.; Luchinat, C. The reaction pathways of zinc enzymes and related biological catalysts. In *Bioinorganic Chemistry*; Bertini, I., Gray, H. B., Lippard, S. J., Valentine, J. S., Eds.; University Science Books: Mill Valley, 1994; pp 37−106.

DOI: 10.1021/jacs.7b01202
J. Am. Chem. Soc. XXXX, XXX, XXX−XXX